Journal of Solid State Chemistry 182 (2009) 1982–1989

Contents lists available at ScienceDirect

Journal of Solid State Chemistry

journal homepage: www.elsevier.com/locate/jssc

On the magnetic structure of $DyNiO_3$

A. Muñoz [a,*], J.A. Alonso [b], M.J. Martínez-Lope [b], M.T. Fernández-Díaz [c]

[a] Dpto. de Física Aplicada, EPS, Universidad Carlos III, Avda. Universidad 30, E-28911, Leganés-Madrid, Spain
[b] Instituto de Ciencia de los Materiales de Madrid, CSIC, E-28049, Cantoblanco-Madrid, Spain
[c] Institut Laue Langevin, B.P. 156, F-38042, Grenoble Cedex 9, France

ARTICLE INFO

Article history:
Received 10 January 2009
Received in revised form
14 April 2009
Accepted 9 May 2009
Available online 18 May 2009

Keywords:
Metal–insulator transition
Charge disproportionation
Antiferromagnetic ordering
Nickel perovskite
Dysprosium nickelate

ABSTRACT

The crystallographic structure of $DyNiO_3$ has been investigated at $T = 200$, 100, and 2 K from high-resolution neutron powder diffraction (NPD) data. We show that the structure is monoclinic, space group $P2_1/n$, from the metal–insulator transition temperature at $T_{MI} = 564$ K down to 2 K. The Ni atoms occupy two different sites 2*d* (Ni1) and 2*c* (Ni2), whose valences, estimated from bond-valence consideration, are +2.43(1) and +3.44(1) at 2 K, respectively. This is interpreted as the result of a partial charge disproportionation of the type $2Ni^{3+} \rightarrow Ni1^{(3-\delta)+} + Ni2^{(3+\delta)+}$, with $\delta \approx 0.55$ at $T = 2$ K. The magnetic structure has been studied from a NPD pattern at $T = 2$ K, well below the establishment of the antiferromagnetic (AFM) ordering at $T_N = 154$ K, as well as from sequential data collected from 16 K down to 2 K. The magnetic order is defined by the propagation vector $\mathbf{k} = (1/2,0,1/2)$. Two possible magnetic structures are compatible with the magnetic intensities. In the second solution both Ni sublattices participate in the magnetic order, as well as Dy since it corresponds to a total disproportionation of Ni^{3+} to Ni^{2+} and Ni^{4+}. In the second solution both Ni sublattices participate in the magnetic order, as well as Dy. The magnetic moments for Ni1 and Ni2 atoms at $T = 2$ K are 1.8 (2) and 0.8 (2) μ_B, respectively. These values are also compatible with a partial charge disproportionation. Dy^{3+} ions exhibit long-range magnetic ordering below 8 K. An abrupt contraction of the unit-cell volume is observed at this temperature, due to a magnetoelastic coupling. The magnetic moment for Dy^{3+} at $T = 2$ K is 7.87 (6) μ_B.

1. Introduction

The family of $RNiO_3$ (R = rare earth and Y) perovskites has been the object of numerous studies in recent times. The most important feature of the $RNiO_3$ oxides is the occurrence of a metal–insulator (MI) transition [1–7] at T_{MI}, evolving with the size of the rare-earth cation, and an antiferromagnetic order transition at $T_N \leq T_{MI}$ giving rise to an unexpected antiferromagnetic structure.

$LaNiO_3$ (space group *R*-3*c*) [4] is the only known compound of the family that remains metallic in all the temperature range. For the other rare-earths the perovskites become metallic above T_{MI} spanning from 130 K for Pr to 559 K for Lu [5]. A first evidence of a charge disproportionation effect ($2Ni^{3+} \rightarrow Ni^{3-\delta} + Ni^{3+\delta}$) coupled to the MI transition was given by diffraction methods for $YNiO_3$ [8], and then for other $RNiO_3$ compounds with smaller R^{3+} cations (R = Ho, Y, Er, Tm, Yb and Lu) [9]. This effect is associated with a structural phase transition from an orthorhombic (*Pbnm*) symmetry in the metallic state above T_{MI}, to a monoclinic symmetry (space group $P2_1/n$) [8,9] below T_{MI}. Soon, some evidences, mainly by spectroscopic techniques indicating that the charge disproportionation phenomenon could be a universal effect for all the members of the $RNiO_3$ series were obtained [9–13].

Let us point out that in the metallic regime, the orthorhombic structure (*Pbnm*) contains four crystallographically equivalent Ni atoms in the unit cell at the 4*b* site. By contrast, in the monoclinic structure ($P2_1/n$), the four Ni atoms of the unit cell are split into two sets of crystallographically independent sites, Ni1 (2*d*) and Ni2 (2*c*) [8], corresponding to alternating large $Ni1O_6$ and small $Ni2O_6$ octahedra. The estimation of the oxidation states of Ni1 and Ni2 in $YNiO_3$ in the insulating phase (at RT) from bond-valence considerations yielded valences of +2.61(1) and +3.17(1) for Ni1 and Ni2 cations, respectively [8], and this is interpreted as a partial charge disproportionation effect that takes place at the MI transition. It was invoked that the negative charge transfer from Ni2 to Ni1 is the driving force for the structural phase transition.

Regarding the magnetic order, the $RNiO_3$ oxides adopt an antiferromagnetic structure defined by the propagation vector $\mathbf{k} = (1/2,0,1/2)$ [3,4,7] at a transition temperature $T_N \leq T_{MI}$. For Pr and Nd, T_N coincides with T_{MI}, but for the rest of the compounds the magnetic ordering temperature occurs below T_{MI}, and the difference between T_N and T_{MI} becomes greater as the size of R is

* Corresponding author.
E-mail address: angel.munoz@uc3m.es (A. Muñoz).

0022-4596/$ - see front matter © 2009 Elsevier Inc. All rights reserved.
doi:10.1016/j.jssc.2009.05.013

reduced. At T_N the magnetic order only concerns the Ni cations, although the magnetic R^{3+} cations become ordered at lower temperatures, as observed for $HoNiO_3$ [14].

For $DyNiO_3$ the MI transition was established at $T_{MI} = 564.1$ K from the anomaly [15] observed in the differential scanning calorimetry (DSC) measurements. In this former study [15], the crystallographic structure of $DyNiO_3$ analysed from neutron diffraction data at room temperature (RT) was considered to be orthorhombic (*Pbnm*). However, a recent investigation [16] of the thermal evolution of the crystallographic structure across T_{MI}, in combination with a Mössbauer study on a Fe-doped sample demonstrates that the crystallographic structure is indeed monoclinic ($P2_1/n$) in the temperature range $RT < T < T_{MI}$. Regarding the magnetic properties of $DyNiO_3$, susceptibility and specific heat measurements [15] showed that Ni cations experience a long-range ordering below $T_N = 154$ K; the order of the Dy^{3+} sublattice was described to take place below 8 K from susceptibility data.

The first aim of this paper is to describe the evolution of the crystallographic structure of $DyNiO_3$ below room temperature from neutron diffraction measurements; we show for the first time, from a low-temperature high-resolution study, that the charge disproportionation of Ni is maintained and even increased down to 2 K. The second aim is to unveil the magnetic structure at $T = 2$ K; we provide with a full Group Theory study of the possible magnetic structures compatible with the monoclinic space group $P2_1/n$, involving the long-range ordering of both Ni and Dy magnetic moments.

2. Experimental measurements

$DyNiO_3$ perovskite was prepared as a polycrystalline powder by high-pressure solid state reactions, as described elsewhere [15]. The neutron powder diffraction (NPD) data were acquired at the Institut Laue-Langevin, Grenoble (France). The crystallographic structure was studied from different patterns collected at the high-resolution D2B two-axis diffractometer with a 1.594 Å wave length. Due to the high neutrons absorption by Dy, the $DyNiO_3$ powder was poured between two concentric vanadium cylinders, minimizing in this way the neutrons path length through the sample. The double-walled vanadium can was put inside of a standard cryostat. In spite of the relatively small amount of sample available (800 mg), good-quality patterns were obtained with counting times of 8 h each in the high-flux mode. The patterns were obtained at $T = 200$, 100 and 2 K. Below the ordering temperature, the same patterns were used to determine the magnetic structure. These data were complemented by a set of neutron diffraction patterns acquired at the D1B multidetector diffractometer with a 2.58 Å wave length. These patterns were sequentially collected every 1 K on heating from 1.5 to 16 K.

The neutron diffraction patterns were analysed by the Rietveld method [17] using the Fullprof program [18]. The peak profile was simulated with a pseudo-Voigt function and the background was fitted by a fifth-degree polynomial function. In the patterns, different Bragg peaks associated with the vanadium sample holder were detected; therefore vanadium metal was considered as a second phase in the final refinement.

3. Experimental results

3.1. Crystallographic structure

The crystallographic structure of $DyNiO_3$ has been refined from the NPD patterns collected at 200, 100 and 2 K with a wave length of 1.594 Å, shown in Fig. 1. The monoclinic $P2_1/n$ structure [16] recently described for the crystallographic structure below

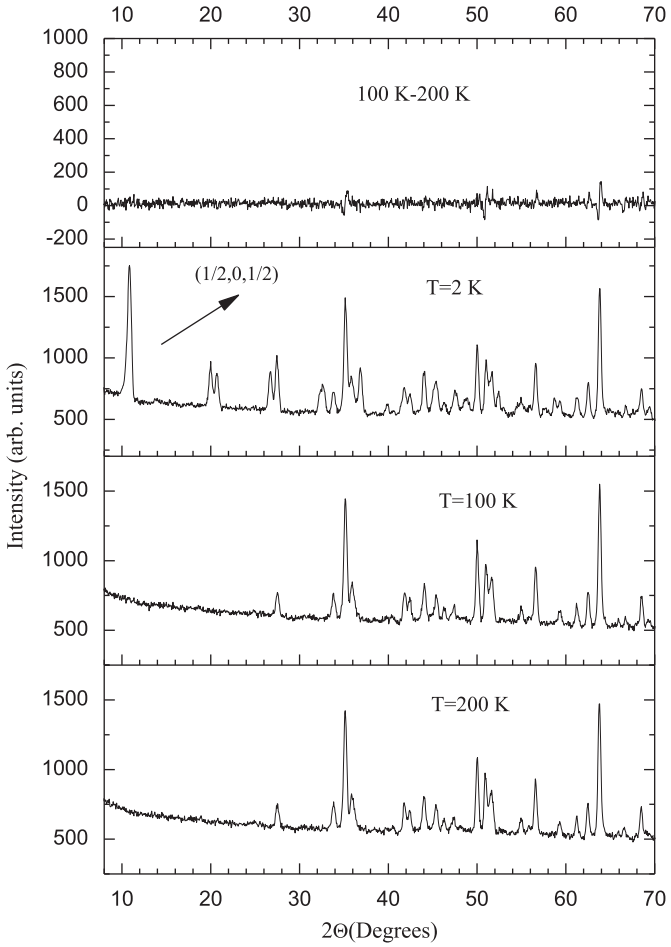

Fig. 1. Neutron powder diffraction patterns collected at 200, 100 and 2 K. The difference between the NPD patterns at 100 and 200 K is also represented.

$T_{MI} = 564$ K has been used as starting model in the refinement. Let us point out that the unit-cell parameters in the monoclinic space group are related to the ideal cubic perovskite lattice parameter $a_0 \approx 3.8$ Å by the relationship $a \approx \sqrt{2}a_0$, $b \approx \sqrt{2}a_0$ and $c \approx 2a_0$. In the space group $P2_1/n$ there are two independent sites for the Ni cations denoted Ni1 and Ni2. The Ni1 and Ni2 cations occupy the 2*d* and 2*c* sites, respectively. There are three independent oxygen atoms, O1, O2 and O3, which are placed at the general 4e positions. The Dy cations are also placed at the 4*e* site. The 2K pattern also contained the magnetic contribution from the AFM structure of $DyNiO_3$, which was also included in the refinement, as indicated in the next subsection.

Figs. 2a, b and 3 show the good agreement obtained between the observed and calculated NPD patterns after the refinements carried out at $T = 200$, 100 and 2 K, respectively. The lattice parameters and the corresponding discrepancy factors are shown in Table 1. The atomic positions and the most important bonding distances and bonding angles associated with the $Ni1O_6$ and $Ni2O_6$ octahedra are presented in Tables 2 and 3, respectively. A schematic view of the crystallographic structure of $DyNiO_3$ is shown in Fig. 4, highlighting that $Ni1O_6$ and $Ni2O_6$ octahedra alternate along the three directions of the space, in such a way that each $Ni1O_6$ octahedra is surrounded by six $Ni2O_6$ octahedra and vice versa.

3.2. Magnetic structure

The resolution of the magnetic structure of $DyNiO_3$ ($T_N = 154$ K) has been performed from a NPD pattern acquired at 2 K with a

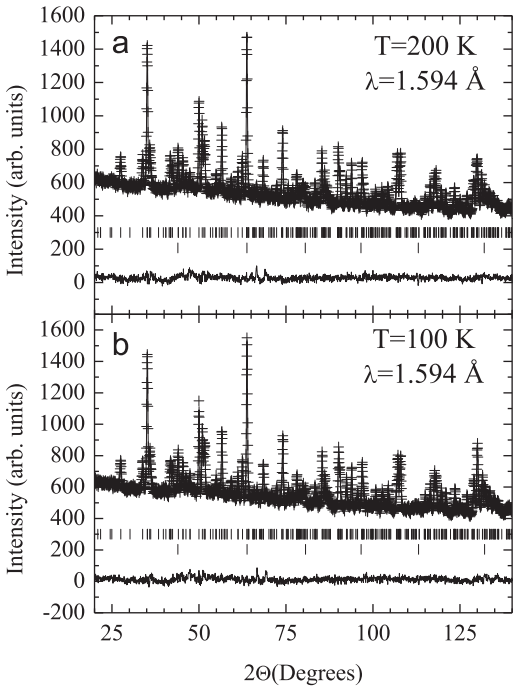

Fig. 2. Comparison of the observed (crosses) and calculated (solid line) NPD patterns at 200 K (a) and 100 K (b). The first and second tick marks correspond to the position of the Bragg reflections of $DyNiO_3$ and of the vanadium sample holder; the line below the tick marks represents the difference between the observed and calculated patterns.

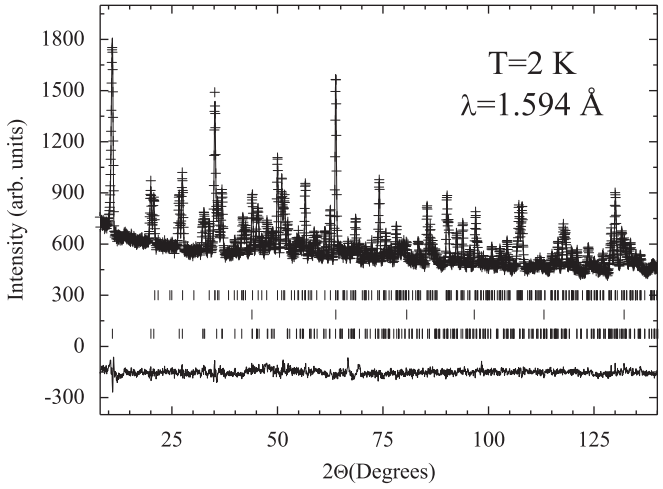

Fig. 3. Comparison of the observed (cross) and calculated (solid line) NPD patterns at $T = 2$ K. The first and second tick marks correspond to the position of the Bragg reflections of $DyNiO_3$ and of the vanadium sample holder; the third tick marks correspond to the magnetic reflections. The difference between the observed and calculated patterns is represented below.

1.594 Å wave length. In the 100 K pattern the magnetic intensities were too weak to be observed (see Fig. 1). In the 2 K pattern, besides the nuclear Bragg reflections associated with the monoclinic crystallographic structure, new peaks connected with the magnetic ordering of $DyNiO_3$ are observed. In fact, the most intense reflection of the diagram, at $2\theta = 10.8^\circ$, has a magnetic origin. All the magnetic reflections could be indexed by using the $\mathbf{k} = (1/2,0,1/2)$ propagation vector. This propagation vector implies a commensurate magnetic unit cell given by $(2a,b,2c)$.

Table 1
Lattice parameters obtained in the Rietveld refinements of the crystallographic structure with $\lambda = 1.594$ Å.

	T (K)		
	200	100	2
a (Å)	5.2063 (1)	5.2059 (1)	5.2062 (2)
b (Å)	5.5073 (1)	5.5063 (1)	5.5067 (1)
c (Å)	7.4382 (2)	7.4305 (2)	7.4277 (2)
β (deg.)	90.027 (9)	90.023 (11)	90.019 (9)
Vol (Å^3)	213.27 (1)	213.00 (1)	212.94 (1)
R_P (%)	2.0	2.1	2.2
R_{wp} (%)	2.6	2.7	2.8
R_{Bragg} (%)	9.4	9.4	6.5
χ^2	1.5	1.6	1.9

Table 2
Atomic positions and isotropic Debye-Waller factors obtained in the structural refinement from NPD data.

		T (K)		
		200	100	2
Dy	4*e* (*x*,*y*,*z*)			
x		0.9820 (4)	0.9814 (4)	0.9820 (5)
y		0.0705 (2)	0.0709 (2)	0.0708 (3)
z		0.250 (2)	0.249 (2)	0.250 (2)
B (Å^2)		0.29 (3)	0.24 (3)	0.30 (4)
Ni1	2*d* (1/2,0,0)			
B (Å^2)		0.58 (4)	0.54 (4)	0.57 (5)
Ni2	2*c* (1/2,0,1/2)			
B (Å^2)		0.58 (4)	0.54 (4)	0.57 (5)
O1	4*e* (*x*,*y*,*z*)			
x		0.0952 (2)	0.0951 (2)	0.0951 (2)
y		0.4740 (2)	0.4734 (2)	0.4738 (2)
z		0.2421 (4)	0.2424 (5)	0.2421 (6)
B (Å^2)		0.51 (6)	0.56 (6)	0.52 (6)
O2	4*e* (*x*,*y*,*z*)			
x		0.7064 (2)	0.7027 (5)	0.7062 (5)
y		0.3066 (5)	0.3087 (5)	0.3063 (6)
z		0.0561 (3)	0.0539 (5)	0.0558 (4)
B (Å^2)		0.51 (6)	0.56 (6)	0.52 (6)
O3	4*e* (*x*,*y*,*z*)			
x		0.1793 (4)	0.1849 (5)	0.1802 (5)
y		0.2060 (5)	0.2090 (5)	0.2058 (6)
z		0.9597 (3)	0.9565 (4)	0.9596 (4)
B (Å^2)		0.51 (6)	0.56 (6)	0.52 (6)

The space group is $P2_1/n$.

In order to determine the possible magnetic structures compatible with the symmetry of $DyNiO_3$, the group theory representation analysis technique described by Bertaut has been followed [19]. For the monoclinic space group $P2_1/n$ and for $\mathbf{k} = (1/2,0,1/2)$, the irreducible representations of the small group $G_{\mathbf{k}}$ are given in Table 4 and they are labelled according to the Kovalev notation [20]. The basis vectors associated with each irreducible representation, determined with the program BasIreps, included in the Fullprof suite [18], are shown in Table 5. The notation for the different sublattices is the following one. For the Ni1 sublattice, the two atoms are denoted as 1 (1/2,0,0) and 2 (0,1/2,1/2); the two atoms of the Ni2 sublattice are named as 3 (0,1/2,0) and 4 (1/2,0,1/2); finally, the four atoms of the Dy sublattice are labelled as 5 (x,y,z), 6 ($-x$+1/2,y+1/2,$-z$+1/2), 7 ($-x,-y,-z$) and 8 (x+1/2,$-y$+1/2,z+1/2).

In most of the cases where several sublattices (Wyckoff sites) are involved in the magnetic order, the magnetic structure is given by the basis vectors of the same irreducible representation for all

Table 3
Main bond distances (Å), distortion parameter Δ_d of the NiO_6 octahedra, bond valences and selected angles (deg.) for $DyNiO_3$.

	T (K)		
	200	100	2
Ni1–O1 (× 2)	1.987 (4)	1.983 (4)	1.984 (4)
Ni1–O2 (× 2)	2.044 (3)	2.041 (3)	2.042 (3)
Ni1–O3 (× 2)	2.041 (2)	2.030 (3)	2.036 (3)
⟨Ni1–O⟩	2.025 (13)	2.018 (3)	2.021 (3)
Δ_d ($\times 10^{-4}$)	1.68	1.55	1.67
B_{VSum} (Ni1)	2.41 (1)	2.45 (1)	2.43 (1)
Ni2–O1 (× 2)	1.873 (4)	1.873 (4)	1.871 (4)
Ni2–O2 (× 2)	1.909 (2)	1.914 (3)	1.910 (3)
Ni2–O3 (× 2)	1.893 (3)	1.897 (3)	1.896 (3)
⟨Ni2–O⟩	1.892 (3)	1.895 (3)	1.892 (3)
Δ_d ($\times 10^{-4}$)	0.61	0.79	0.73
B_{VSum} (Ni2)	3.44 (1)	3.41 (1)	3.44 (1)
Ni1–O1–Ni2	148.96 (15)	148.91 (15)	148.93 (15)
Ni1–O2–Ni2	146.81 (10)	146.66 (11)	146.95 (12)
Ni1–O3–Ni2	148.85 (10)	149.53 (11)	148.96 (12)

The distortion parameter Δ_d for NiO_6 octahedra with an average Ni–O distance ⟨d⟩ is defined as $\Delta_d = (1/6)\Sigma_{n=1,6}[(d_n - \langle d\rangle)/\langle d\rangle]^2$.

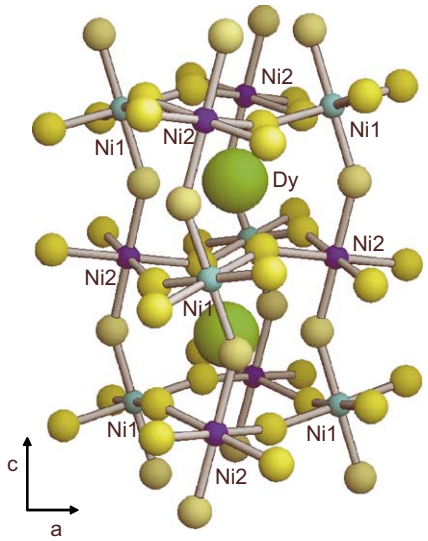

Fig. 4. Schematic view of the crystallographic structure.

the sublattices. In $DyNiO_3$, according to Table 5, it would mean that the magnetic order is due either to the sublattices Ni1 and Dy (τ_1 and τ_3) or to the sublattices Ni2 and Dy (τ_2 and τ_4). It is worthwhile comparing the possible magnetic structures obtained by the group theory for $DyNiO_3$ with those obtained for the former members of the $RNiO_3$ family (R = Pr, Nd) [6,7], following a similar procedure. A *Pbnm* orthorhombic symmetry has been described for these compounds, for which the scenario is more complex since the irreducible representations are two-dimensional. Regarding the Ni atoms, all of them belong to the same Wyckoff site, but according to the basis vectors, the possible magnetic structures can be of both equal moment and non-equal moment. For the R (rare-earth) sublattice, the four atoms are divided into two orbits each of them formed by two atoms; therefore solutions with non-equal moment are possible. This is not the case for $DyNiO_3$, since, according to Table 5, all Dy atoms will have the same magnetic moment and both Ni sublattices participate in the magnetic order. Let us note that in the final magnetic structure reported for the former members of the $RNiO_3$ family [6,7] both Ni sublattices are described to participate in the

Table 4
Irreducible representations of the small group $G_{\mathbf{k}}$ obtained from the space group $P2_1/n$ for $\mathbf{k} = (1/2,0,1/2)$.

	1/(0,0,0)	2y/(1/2,1/2,1/2)	$\bar{1}$/(0,0,0)	$\bar{1}$2y/(1/2,1/2,1/2)
τ_1	1	1	1	1
τ_2	1	1	−1	−1
τ_3	1	−1	1	−1
τ_4	1	−1	−1	1

Table 5
Basis vectors for $DyNiO_3$.

	Ni1 (2d)		Ni2 (2c)		Dy (4e)			
	1	2	3	4	5	6	7	8
τ_1			$\begin{pmatrix}1\\1\\1\end{pmatrix}$	$\begin{pmatrix}\bar{1}\\1\\\bar{1}\end{pmatrix}$	$\begin{pmatrix}1\\1\\1\end{pmatrix}$	$\begin{pmatrix}\bar{1}\\1\\\bar{1}\end{pmatrix}$	$\begin{pmatrix}1\\1\\1\end{pmatrix}$	$\begin{pmatrix}\bar{1}\\1\\\bar{1}\end{pmatrix}$
τ_2	$\begin{pmatrix}1\\1\\1\end{pmatrix}$	$\begin{pmatrix}\bar{1}\\1\\\bar{1}\end{pmatrix}$			$\begin{pmatrix}1\\1\\1\end{pmatrix}$	$\begin{pmatrix}\bar{1}\\1\\\bar{1}\end{pmatrix}$	$\begin{pmatrix}\bar{1}\\1\\\bar{1}\end{pmatrix}$	$\begin{pmatrix}1\\1\\1\end{pmatrix}$
τ_3			$\begin{pmatrix}1\\1\\1\end{pmatrix}$	$\begin{pmatrix}1\\\bar{1}\\1\end{pmatrix}$	$\begin{pmatrix}1\\1\\1\end{pmatrix}$	$\begin{pmatrix}1\\\bar{1}\\1\end{pmatrix}$	$\begin{pmatrix}1\\1\\1\end{pmatrix}$	$\begin{pmatrix}1\\\bar{1}\\1\end{pmatrix}$
τ_4	$\begin{pmatrix}1\\1\\1\end{pmatrix}$	$\begin{pmatrix}1\\\bar{1}\\1\end{pmatrix}$			$\begin{pmatrix}1\\1\\1\end{pmatrix}$	$\begin{pmatrix}1\\\bar{1}\\1\end{pmatrix}$	$\begin{pmatrix}\bar{1}\\\bar{1}\\\bar{1}\end{pmatrix}$	$\begin{pmatrix}\bar{1}\\1\\\bar{1}\end{pmatrix}$

magnetic moment and they exhibit the same magnetic moment value.

In the macroscopic susceptibility measurements reported for $DyNiO_3$ [15], the large paramagnetic signal of Dy^{3+} prevents to conclude if both Ni lattices are involved in the magnetic ordering below $T_N = 154$ K, although it seems clear that the ordering of the Dy sublattice is only established below 8.5 K. Nevertheless, our neutron data clearly show that the periodicity of the magnetic order associated with the Dy sublattice is also given by the propagation vector $\mathbf{k} = (1/2,0,1/2)$.

Therefore, the possibility that both Ni sublattices participate in the magnetic order has also been taken into consideration upon resolving the magnetic structure. This assumption implies a mixture of the basis vector belonging to different irreducible representations. The combinations that have been considered have been $\tau_1+\tau_2$, $\tau_1+\tau_4$, $\tau_2+\tau_3$ and $\tau_3+\tau_4$.

As mentioned before, although the Ni sublattice of $DyNiO_3$ is already ordered at $T = 100$ K, the magnetic peaks are not observed since the ordered magnetic moments on the Ni sites at this temperature are still too weak, below the detection threshold for neutrons. This can clearly be observed in Fig. 1, in which the difference between the NPD patterns acquired at $T = 100$ K and $T = 200$ K is represented. Therefore, the resolution of the magnetic structure has been carried out from the 2 K NPD data, taking into account that at this temperature the Dy sublattice is also ordered.

After checking the different magnetic structure models, two solutions have been found to be compatible with the experimental data. For the first solution, the basis vectors belong to the same irreducible representation, τ_2, which implies that only the Ni1 and Dy sublattices participate in the magnetic ordering. The coupling of the magnetic moments of the atoms for the Ni1 sublattice is $m_{1x} = -m_{2x}$, $m_{1y} = m_{2y}$ and $m_{1z} = -m_{2z}$; for the Dy sublattice the coupling is $m_{5x} = -m_{6x} = -m_{7x} = m_{8x}$, $m_{5y} = m_{6y} = -m_{7y} = -m_{8y}$, and $m_{5z} = -m_{6z} = -m_{7z} = m_{8z}$, which

Table 6
Results of the magnetic structure resolution at $T = 2$ K.

	Ni1	Ni2	Dy
Solution 1	τ_2	τ_2	τ_2
(m_x,m_y,m_z) (μ_B)	(1.4 (2), 1.1 (1), 0)	–	(3.6 (1), 6.86 (7), −1.4 (1))
$\|m\|$ (μ_B)	1.7 (2)	–	7.87 (6)
R_{Bmagn}		11.0	
Solution 2	τ_2	τ_1	τ_2
(m_x,m_y,m_z) (μ_B)	(1.53 (5), −0.95 (8), 0)	(0.68 (2), −0.43 (3), 0)	(3.4 (1), 6.75 (6), −1.4 (1))
$\|m\|$ (μ_B)	1.8 (2)	0.8 (2)	7.67 (5)
R_{Bmagn}		11.0	

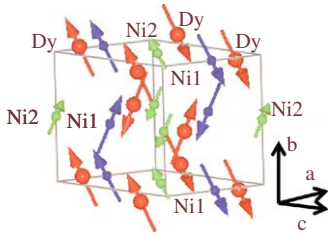

Fig. 5. A view of the magnetic structure (solution 2) where Ni1, Ni2 and Dy are all involved in the magnetic ordering, at $T = 2$ K.

corresponds to the basis vectors (A_x,C_y,A_z). The magnetic moment values obtained in the fitting are shown in Table 6.

The second solution corresponds to a mixture of the basis functions of the irreducible representations τ_1 and τ_2. The coupling of the magnetic moments for the Ni1 and Dy sublattices is the same as in the first solution, and the coupling for the Ni2 sublattice corresponds to the basis vectors of τ_1. Therefore, it implies $m_{3x} = -m_{4x}$, $m_{3y} = m_{4y}$ and $m_{3z} = -m_{4z}$. The magnetic moments values obtained in the fitting are also shown in Table 6. Let us point out that, as regarding the orientation of the magnetic moments for both Ni sublattices, the best agreement is achieved when the orientation of the magnetic moments of the Ni1 sublattice is collinear with the magnetic moments of the Ni2 sublattice within each (0 0 1) layer. The observed NPD pattern and the calculated one for the second solution (both Ni sublattices as well as Dy sublattice are ordered) are compared in Fig. 3. A view of the orientation of the magnetic moments in the unit cell for the second solution is shown in Fig. 5. Whereas the magnetic moments of the Ni atoms are in the (0 0 1) plane (the z-component is zero), the magnetic moments of the Dy sublattice present the three components. Both solutions show similar agreement R_{mag} factors. More detailed views of the arrangements of the Ni moments for both solutions are shown in Figs. 6 and 7.

In order to elucidate if, in a certain way, it is possible to discriminate between the two solutions, we have applied Hamilton's R-factor test [21]. In this case, there are 782 observations (number of magnetic reflections considered in the fitting), and, for the solutions 1 and 2, the number of parameters considered to fit the magnetic contribution of the pattern have been, respectively 18 and 21. So, according to Hamilton's criterion, we must compare $R_{1,782,0.5}$ with R_{Mag2}/R_{Mag1} (the magnetic R-factor corresponding to solutions 2 and 1). In our case $R_{1,782,0.5} = 1.0011$ and $R_{Mag2}/R_{Mag1} = 1 = R$ so, as R and $R_{1,782,0.5}$ as nearly equal, if solution 2 is rejected the probability of error would be 50%. Therefore, it is not possible to choose one of the solutions after applying Hamilton's criterion.

The arrangement of the magnetic moments has also been analysed from a set of NPD patterns collected in the temperature range1.5–16 K with a 2.58 Å wave length. The thermal evolution of

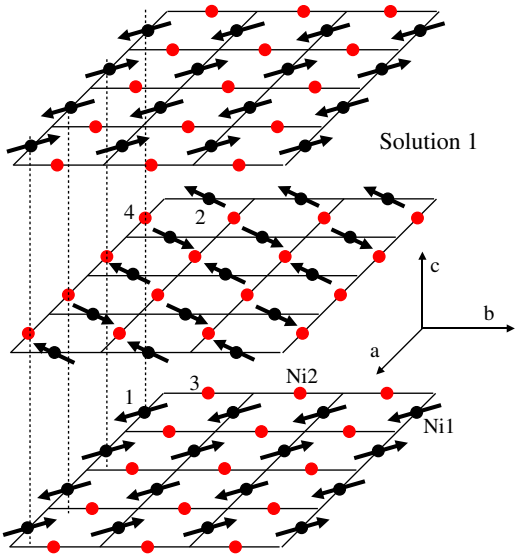

Fig. 6. Schematic view of the arrangement of Ni moments for solution 1.

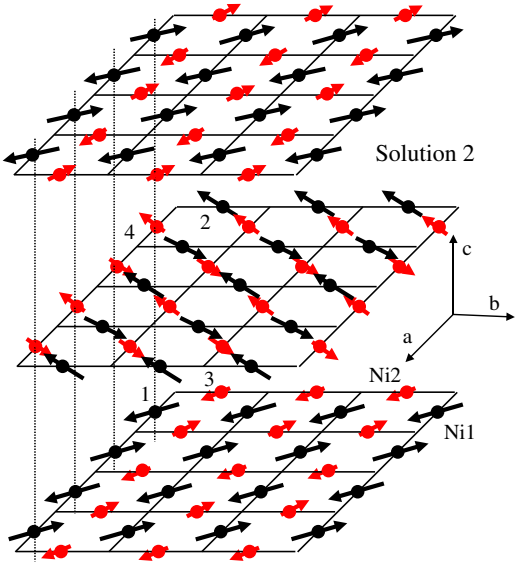

Fig. 7. Schematic view of the arrangement of Ni moments for solution 2.

the NPD patterns is shown in Fig. 8; an important increase of the intensity of the magnetic reflections can be appreciated below 8 K, in particular the (1/2,0,1/2) reflection. This is associated with the onset of the magnetic order in the Dy sublattice. After considering the different magnetic solutions below 8 K, the best fitting is again achieved for the solutions 1 and 2, as obtained with the NPD

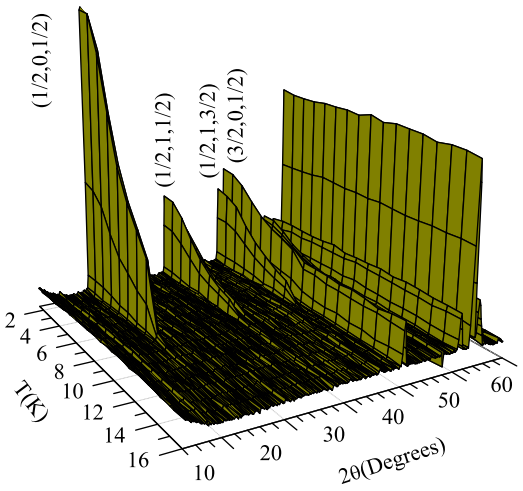

Fig. 8. Thermal evolution of the NPD patterns acquired with a 2.58 Å wave length between 1.5 and 16 K.

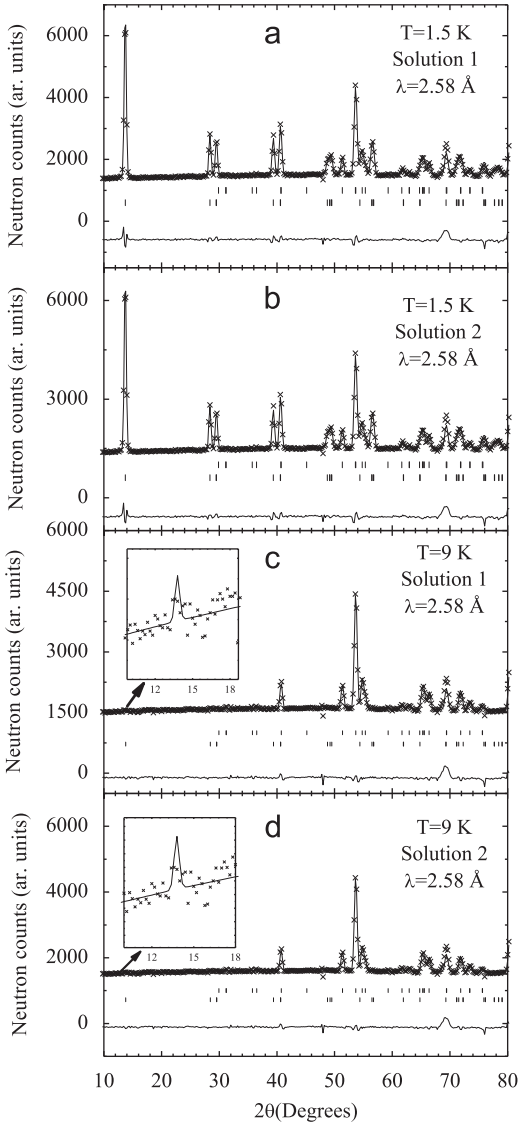

Fig. 9. Comparison of the observed (cross) and calculated (solid line) NPD patterns at $T = 1.5$ K for solution 1 (a) and solution 2 (b) and for $T = 9$ K for solutions 1 (c) and 2 (d). The first tick marks correspond to the position of the Bragg reflections of $DyNiO_3$ and the second tick marks correspond to the magnetic reflections. The difference between the observed and calculated patterns is represented below.

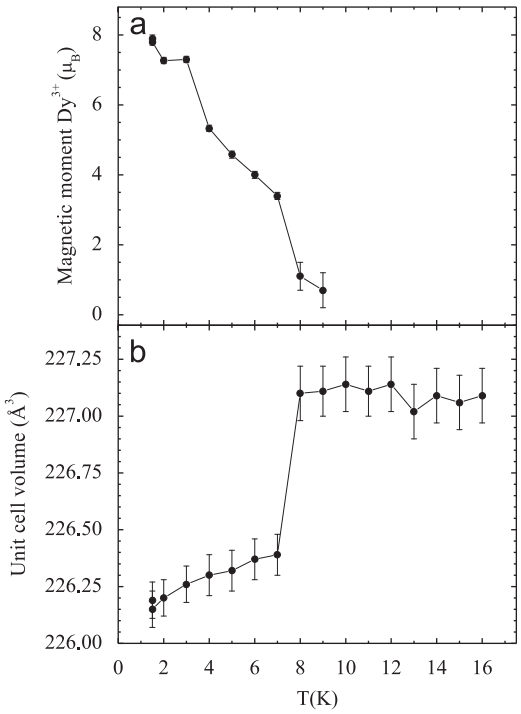

Fig. 10. Thermal evolution of the magnetic moments for the Dy sublattice (a) and of the unit cell volume (b).

patterns collected with $\lambda = 1.594$ Å. The good agreement between the calculated and observed NPD patterns for both solutions at 1.5 K can be seen in Fig. 9. In this case the corresponding R_{mag} factors are 6.6 and 6.7 for the solutions 1 and 2, respectively. So by considering Hamilton's *R*-factor test [21] it is not possible to reject one of the solutions. In Fig. 9, the fitting of the pattern obtained at 9 K has also been included; in this case only the order of the Ni sublattices has been taken into consideration. It can be appreciated that the intensity of the magnetic peaks can be hardly distinguished from the background, partially because a strong incoherent scattering is coming from paramagnetic Dy moment.

The thermal evolution of the magnetic moment for the Dy^{3+} magnetic moment is shown in Fig. 10a; according to the figure, the magnetic order of the Dy sublattice takes place at around 8 K. Fig. 10b shows the thermal evolution of the unit-cell volume. There is an abrupt contraction of the volume from 227.1 $Å^3$ at 8 K to 226.4 $Å^3$ at 7 K, coinciding with the onset of the magnetic order in the Dy sublattice, which suggests a strong magnetoelastic effect in this compound, which had not been described before for any member of the $RNiO_3$ perovskite family.

4. Discussion

A recent study [16] of the crystallographic structure evolution across the T_{MI} transition in $DyNiO_3$ has disclosed that, below $T_{MI} = 564$ K, the structure is monoclinic, space group $P2_1/n$. In complement, in the present work we show that the monoclinic structure remains stable down to 2 K. In the monoclinic structure the Ni atoms occupy two different sites 2*d* (Ni1) and 2*c* (Ni2), both being octahedrally coordinated; the large $Ni1O_6$ and small $Ni2O_6$ octahedra alternate along the {0 0 1} and {1 1 0} directions sharing a common oxygen. At RT [16], the average ⟨Ni1–O⟩ distance (2.010(11) Å) is considerably larger than ⟨Ni2–O⟩ distance (1.910(11) Å). This fact is also verified below RT; for instance, at $T = 2$ K the average ⟨Ni1–O⟩ and ⟨Ni2–O⟩ distances are

2.021(3) and 1.892(3) Å, suggesting an even greater charge disproportionation effect.

Another important parameter to be considered is the distortion of the NiO_6 octahedra, defined by $\Delta_d = (1/6)\sum_{n=1}^{6}[(d_n - \langle d \rangle)/\langle d \rangle]^2$. For all the temperatures the $Ni1O_6$ octahedron is more distorted than the $Ni2O_6$ octahedron, as already observed at RT [16]. For instance, the distortion Δ_d at $T = 2$ K are 1.67×10^{-4} and 0.73×10^{-4} for $Ni1O_6$ and $Ni2O_6$ octahedra, respectively. There is no significant evolution of these distortion values in the considered temperature range. In order to determine the valence of the Ni1 and Ni2 ions, we have used the phenomenological Brown's bond-valence model [22]. This model allows us to estimate the Ni valence in the ionic limit from the Ni–O bonding distances. The valence is the sum of the individual bond valences (s_i) for Ni–O bonds; the individual bond valences are calculated as $s_i = \exp[(r_0 - r_i)/B]$; $B = 0.37$, $r_0 = 1.686$ for the Ni^{3+}–O^{2-} pair. The r_0 value for Ni^{3+} has been considered for both Ni sublattices. At $T = 2$ K the valence for the Ni1 and Ni2 ions are +2.43(1) and +3.44(1) valence units, respectively. Again, there is no noticeable evolution of the Ni valences in this temperature interval. If, as in the case of $YNiO_3$ [8] it is assumed that we are in the presence of a charge disproportionation effect of the type $2Ni^{3+} \rightarrow Ni1^{(3-\delta)+} + Ni2^{(3+\delta)+}$, at 2 K we would have $\delta \approx 0.52$. As we commented above, this is significantly higher than the value observed at RT, $\delta \approx 0.38$ [11]. Also at 2 K, this δ value implies that the charge disproportionation is not complete ($2Ni^{3+} \rightarrow Ni1^{2+} + Ni2^{4+}$), although it is greater than that observed in other Ni perovskites at RT, such as $HoNiO_3$ [9] and $YNiO_3$ [8], for which we have $\delta \approx 0.30$ and ≈ 0.35, respectively. Let us point out that the charge disproportionation implies a charge transfer between two NiO_6 octahedra. To a certain extent, the fact that a single type of NiO_6 octahedra at the orthorhombic, metallic phase, splits into two non-equivalent $Ni1O_6$ and $Ni2O_6$ octahedra upon the charge localization at T_{MI}, with a different distortion and a different valence, has suggested that the charge disproportionation is the driving force of the T_{MI} transition. However, Zhou and Goodenough [23] have interpreted this behaviour within a different approach, upon observing that, below the T_{MI} transition, the more distorted the NiO_6 octahedra, the longer the Ni–O bonding distances. Furthermore, a greater distortion of the $Ni1O_6$ octahedron is associated with a major presence of the Jahn–Teller effect. On comparing the average bonding distances Ni–O in the $Ni1O_6$ and $Ni2O_6$ octahedra with the corresponding M–O bonding distances in the RMO_3 compounds (M = Fe and Ni), Zhou and Goodenough [23] concluded that the Ni1–O bonds are mainly ionic whereas the Ni2–O bonds exhibit a covalent character. The distortion originated by the Jahn–Teller effect is enhanced in an ionic Ni–O bonding while it is reduced in case of a covalent Ni–O bonding. In this way, according to Goodenough's interpretation, instead of a real charge transfer between NiO_6 octahedra, a segregation into ionic and covalent bonding would take place due to cooperative oxygen displacements.

It is interesting to discuss the two alternative solutions found for the magnetic ordering of $DyNiO_3$ at 2 K, represented in Figs. 6 and 7 for the Ni sublattices. In the first solution (Fig. 6), only the Ni1 and Dy sublattices are involved in the magnetic ordering, the Ni2 atoms showing no ordered magnetic moment. It can be observed that along the [1 1 0], [1 $\bar{1}$ 0] and [0 0 1] directions the coupling between the closer Ni1 ions is antiferromagnetic (AF). This magnetic structure would be possible for a complete charge disproportionation and therefore, the electronic configuration for the Ni1 and Ni2 atoms were d^8 and d^6, respectively. For this solution, the magnetic moment found for the Ni1 atoms is 1.7(2) μ_B, which suggests for the Ni1 atoms the electronic configuration $t_{2g}^6 e_g^2$ ($S = 1$) as the ground state, and for the Ni2 atoms in the low-spin configuration, the electronic configuration is $t_{2g}^6 e_g^0$ ($S = 0$). The ordered magnetic moment for Dy^{3+} is 7.87(6) μ_B in this first solution.

According to Fig. 7, the magnetic structure corresponding to the second solution can be described in the following way. Within the (0 0 1) planes the magnetic moments of the Ni1 atoms are collinearly oriented with respect to the magnetic moments of the Ni2 atoms. Along the [0 0 1] direction the arrangement of the magnetic moments in the $z = 0$ and $z = 1$ planes is also collinear, but the magnetic moments at the $z = 1/2$ plane are not parallel to those of $z = 0$; this is due to the fact that the magnetic space group is $P2_1$. Let us recall that this solution is a combination of the basis vectors associated with the τ_1 and τ_2 irreducible representations whose magnetic space groups are $P2_1/n$ and $P2_1/n'$, respectively. As seen in Fig. 7 along the [1 1 0] and [1 $\bar{1}$ 0] directions, the magnetic coupling for the sequence Ni1–Ni2–-Ni1–Ni2–Ni1 is AFM–FM–AFM–FM, where FM denotes a ferromagnetic coupling. This same coupling is also observed along the [0 0 1] direction, although for the x-component of the magnetic moments the coupling is AFM–FM–AFM–FM and for the y-component it is FM–AFM–FM–AFM. This second solution is compatible with a partial charge disproportionation as determined in the structural analysis and it implies a magnetic coupling similar to the coupling observed for the former members of the $RNiO_3$ family as R = Pr, Nd, Sm and Eu [6,7].

For the second solution the magnetic moments for the Ni1 and Ni2 atoms at $T = 2$ K are 1.8(2) and 0.8(2) μ_B, respectively. As mentioned before, the valences for the Ni1 and Ni2 ions are +2.43(1) and +3.44(1), respectively. The large magnetic moment value obtained for Ni1 is compatible with the electronic injection on e_g orbitals resulting from the partial charge disproportionation; for $\delta \approx 0.52$ a magnetic moment of 1.52 μ_B would be expected for Ni1, within the standard deviation of the observed moment. For $Ni2^{(3+\delta)+}$ ions the ground state is low spin $t_{2g}^6 e_g^1$ (Ni^{3+}), with a moment reduction owing to the mentioned electronic transfer. Let us point out that the anisotropy of the Ni–O bonding distances observed in $Ni1O_6$ octahedra can be responsible for the lack of colinearity of the orientation of the magnetic moments in the $z = 0$ and $z = 1/2$ planes, since the Ni–O bonding distances along the [0 0 1] direction, Ni1–O1 and Ni2–O1 are significantly smaller than the Ni–O distances within the (0 0 1) plane.

Concerning the magnetic ordering of the Dy sublattice, with an ordered magnetic moment of 7.67(5) μ_B, the periodicity of the magnetic structure is also given by the propagation vector $\mathbf{k} = (1/2,0,1/2)$. This result contrasts with previous reports for $RNiO_3$ perovskites with magnetic rare-earths; in $NdNiO_3$ it was found that Nd^{3+} moments remain paramagnetic, whereas in $HoNiO_3$ [14] the Ho sublattice becomes ordered with a different propagation vector $\mathbf{k} = 0$. In our case, the similar periodicity observed suggests that the Dy^{3+}–O–Ni^{3+} interactions are predominant over the Dy^{3+}–O–Dy^{3+} superexchange interactions, since the rare earth sublattice and the transition metal sublattice are clearly coupled. A similar behaviour has been found in some multiferroic compounds, e.g., $TbMNO_3$ and $DyMnO_3$ [24]. In this case the influence of the exchange interaction J_{R-Mn} has been analysed by considering a one-dimensional ANNNI Ising model. According to this model, a weak R–Mn coupling implies that the propagation vector $\mathbf{k}$ of the R and Mn ordering are decoupled, whereas a high value of the J_{R-Mn} parameter implies a strong coupling of the R and Mn ordering.

5. Summary and conclusions

The NPD study of the crystallographic structure of $DyNiO_3$ below RT, in complement with the previous investigation above RT, shows that the structure is monoclinic, space group $P2_1/n$,

from the metal–insulator transition temperature at $T_{MI} = 564$ K down to 2 K. Large $Ni1O_6$ and small $Ni2O_6$ octahedra alternate along the [1 1 0], [1 $\bar{1}$ 0] and [0 0 1] directions. $Ni1O_6$ octahedra show a considerably higher distortion than $Ni2O_6$. According to the phenomenological Brown's bond valence model, the valence for the Ni1 and Ni2 ions at $T = 2$ K are +2.43(1) and +3.44(1), respectively. This is the result of a partial charge disproportionation of the type $2Ni^{3+} \rightarrow Ni1^{(3-\delta)+} + Ni2^{(3+\delta)+}$ in $DyNiO_3$, as it has previously been observed for $YNiO_3$ and other members of the $RNiO_3$ family. We show for the first time, from a low-temperature high-resolution study in $RNiO_3$ perovskites, that the charge disproportionation of Ni is maintained and even increased down to 2 K.

The magnetic structure has been studied from a NPD pattern at $T = 2$ K, well below the establishment of the antiferromagnetic ordering of the Ni sublattice at $T_N = 154$ K, and also below the magnetic ordering of the Dy sublattice at 8 K. The propagation vector $\mathbf{k} = (1/2,0,1/2)$ is the same as the one encountered for the Ni sublattice in other members of the $RNiO_3$ family (R = Pr, Nd, Ho, Y). The same propagation vector is associated with the Ni1, Ni2 and Dy sublattices of $DyNiO_3$. Two different magnetic structures have been found to be compatible with the experimental data. In the first solution only the Ni1 and Dy sublattices are long-range ordered, the magnetic structure being defined by the basis vectors belonging to the τ_2 irreducible representation. Concerning the Ni1 sublattice, the magnetic moments are AFM coupled along the [1 1 0], [1 $\bar{1}$ 0] and [0 0 1] directions. The second solution of the magnetic structure is given by a combination of the basis vectors of the τ_1 and τ_2 irreducible representations. In this case both Ni sublattices as well as the Dy sublattice participate in the magnetic order. Along [1 1 0], [1 $\bar{1}$ 0] and [0 0 1] directions, the magnetic coupling along the sequence Ni1–Ni2–Ni1–Ni2–Ni1 is AFM–FM–AFM–FM. This magnetic structure is compatible with the partial charge disproportionation observed in the crystal structure. Unlike $HoNiO_3$, where the Ho sublattice becomes ordered with a different propagation vector $\mathbf{k} = 0$, in $DyNiO_3$ the periodicity of the Dy magnetic structure is also given by the propagation vector $\mathbf{k} = (1/2,0,1/2)$, suggesting that the Dy^{3+}–Dy^{3+} superexchange coupling is less important than the Dy^{3+}–Ni^{3+} exchange interactions. The unit cell volume undergoes a sudden contraction at 8 K, concomitant with the onset of long-range magnetic ordering for Dy^{3+} moments, suggesting a strong magnetoelastic effect.

References

[1] P. Lacorre, J.B. Torrance, J. Pannetier, A.I. Nazzal, P.W. Wang, T.C. Huang, J. Solid State Chem. 91 (1991) 225.
[2] J.B. Torrance, P. Lacorre, A.I. Nazzal, E.J. Ansaldo, C. Niedermayer, Phys. Rev. B 45 (1992) 8209.
[3] M. Medarde, J. Phys.: Condens. Matter 9 (1997) 1679.
[4] J.L. García-Muñoz, J. Rodríguez-Carvajal, P. Lacorre, J.B. Torrance, Phys. Rev. B 46 (1992) 4414.
[5] J.A. Alonso, M.J. Martínez-Lope, M.T. Casais, J.L. García-Muñoz, M.T. Fernández-Díaz, M.A.G. Aranda, Phys. Rev. B 64 (2001) 94102.
[6] J.L. García-Muñoz, J. Rodríguez-Carvajal, P. Lacorre, Phys. Rev. B 50 (1994) 978–991.
[7] J. Rodríguez-Carvajal, S. Rosenkranz, M. Medarde, P. Lacorre, M.T. Fernández-Díaz, F. Fauth, V. Trounov, Phys. Rev. B 57 (1998) 456–464.
[8] J.A. Alonso, J.L. García-Muñoz, M.T. Fernández-Díaz, M.A.G. Aranda, M.J. Martínez-Lope, M.T. Casais, Phys. Rev. Lett. 82 (1999) 3871–3874.
[9] J.A. Alonso, M.J. Martínez-Lope, M.T. Casais, J.L. García-Muñoz, M.T. Fernández-Díaz, Phys. Rev. B 61 (2000) 1756–1763.
[10] U. Staub, G.I. Meijer, F. Fauth, R. Allenspach, J.G. Bernorz, J. Karpinski, S.M. Kazakov, L. Paolasini, F. D'Acapito, Phys Rev. Lett. 88 (2002) 126402.
[11] C. Piamonteze, H.C.N. Tolentino, A. Ramos, N.E. Massa, J.A. Alonso, M.J. Martínez-Lope, M.T. Casais, Phys. Rev. B 71 (2005) 012104.
[12] A. Caytuero, H. Micklitz, M.M. Abd-Elmeguid, F.J. Litterst, J.A. Alonso, A. Baggio-Saitovitch, Phys. Rev. B 76 (2007) 193105.
[13] M. Acosta-Alejandro, J. Mustre de León, M. Medarde, Ph. Lacorre, K. Konder, P.A. Montano, Phys. Rev. B 77 (2008) 085107.
[14] M.T. Fernández-Díaz, J.A. Alonso, M.J. Martínez-Lope, M.T. Casais, J.L. García-Muñoz, Phys. Rev. B 64 (2001) 144417.
[15] J.A. Alonso, M.J. Martínez-Lope, M.T. Casais, J.L. Martínez, G. Demazeau, A. Largeteau, J.L. García-Muñoz, A. Muñoz, M.T. Fernández-Díaz, Chem. Mater. 11 (1999) 2463–2469.
[16] J.A. Alonso, M.J. Martínez-Lope, G. Demazeau, M.T. Fernández-Díaz, I.A. Presniakov, V.S. Rusakov, T.V. Gubaidulina, A.V. Sobolev, Dalton Trans. (2008).
[17] H.M. Rietveld, J. Appl. Crystallogr. 2 (1969) 65.
[18] J. Rodríguez-Carvajal, J. Phys. B 192 (1993) 55.
[19] E.F. Bertaut, in: G.T. Rado, H. Shul (Eds.), Magnetism, vol. III, Academic Press, New York, 1963 (Chapter 4).
[20] O.V. Kovalev, in: H.T. Stokes, D.M. Hatch (Eds.), Representation of Crystallographic Space Groups: Irreducible Representations, Induced Representation and Corepresentations, Gordon and Breach Science Publishers, 1993.
[21] W.C. Hamilton, Acta Crystallogr. 18 (1965) 502.
[22] I.D. Brown, in: M. O'Keefe, A. Navrotsky (Eds.), Structure and Bonding in Crystals, vol. 2, Academic Press, New York, 1981, pp. 1–30.
[23] J.-S. Zhou, J.B. Goodenough, Phys. Rev. B 69 (2004) 153105.
[24] O. Prokhnenko, R. Feyerherm, M. Mostovoy, N. Aliouane, E. Dudzik, A.V.B. Wolter, A. Maljuk, D.N. Argyriou, Phys. Rev. Lett. 99 (2007) 177206.